Hindawi
International Journal of Antennas and Propagation
Volume 2021, Article ID 9926753, 9 pages
https://doi.org/10.1155/2021/9926753

Research Article

A Novel Multiband Fractal Antenna for Wireless Application

Lan Wang, Jianguo Yu, Tangyao Xie, and Kun Bi

Beijing Key Laboratory of Work Safety Intelligent Monitoring (Beijing University of Posts and Telecommunications), Beijing, China

Correspondence should be addressed to Lan Wang; 1879426363@qq.com and Jianguo Yu; yujianguo241401@163.com

Received 25 March 2021; Revised 28 April 2021; Accepted 3 June 2021; Published 17 June 2021

Academic Editor: Taimoor Khan

This paper proposes a novel multiband antenna using circle and triangle fractals for wireless application. By cutting a triangle slot in the circular monopole, a novel fractal method of the circular nested triangle structure is presented. The above structure is iterated four times, which forms the proposed fractal antenna. The antenna adopts the microstrip feeding method. In order to improve out band rejection and expand bandwidth, a ring resonator is designed on the back of the dielectric plate. The designed antenna covers 1.8 GHz–2.9 GHz applied to Bluetooth, TD-SCDMA, WCDMA, CDMA2000, and LTE33-41, 3.4 GHz–4.6 GHz applied to LTE 42/43 and WiMAX, and 5 GHz–5.6 GHz applied to WLAN. The substrate is FR4 with a dielectric constant of 4.4 and a loss tangent of 0.02. The size of the fabricated antenna is $87.5 \times 61 \times 1.6$ mm. The measured pick gain achieves 2.98 dBi, 2.58 dBi, and 3.34 dBi at 2.6 GHz, 3.8 GHz, and 5.3 GHz, respectively. The measurement and simulation results are in good agreement, which verifies the rationality of the design.

1. Introduction

With the advancement of wireless communication technology, multiband antenna has played a very crucial role in the wireless personal area network [1–9]. Mobile devices, such as hand-held computers and smart phones, are widely using wireless local area network (WLAN) and worldwide interoperability for microwave access (WiMAX) [10–14]. The WLAN/WiMAX module, used to avail of these environments, is capable of operating at multiple frequency bands. The typical frequency bands required for a single antenna are therefore 2.4, 5.2, 5.4, and 5.8 GHz for WLAN applications, 3.3–3.8 GHz for WiMAX, and 2.4–2.484 GHz for Bluetooth applications [15–18]. The use of printed technology is the best choice since it allows to design low-cost planar antennas with high performances and compact size. Moreover, a printed antenna can be easily integrated into front-end circuits, providing low profile and a relatively simple fabrication [3, 19–21]. Therefore, a number of printed antennas with different geometries have been experimentally characterized to enhance the bandwidth for wireless applications. In the work by Gautam et al. [22], a low-profile planar triple-band microstrip antenna was used for WLAN/WiMAX applications. The proposed antenna consists of F-shaped slot radiators and a defected ground plane. In the work by Augustin and Denidni [23], a multiband trapezoidal monopole antenna is proposed, which is fed by coplanar waveguide (CPW). Linear and circular polarizations are realized in a single substrate layer. In the work by Li and Mao [24], a novel Koch-like fractal curve is proposed. A small isosceles triangle is cut off from center of each side of the initial isosceles triangle; then, the procedure iterates along the sides like Koch curve does, forming the Koch-like fractal bowtie geometry. In the study by Liu et al. [25], an optically controlled aperture ultrawideband antenna is presented, which is able to generate reconfigurable multiband notches. Two independent narrow-band complementary split ring resonators are controlled by two optically controlled microwave switches. In the work by Kunwar et al. [26], inverted L-slot patch with a defected ground plane is used for triple-band operation. A frequency-agile triple-band microstrip antenna using the defected ground structure is presented in [27]. MTM-inspired reactive loading and metamaterial transmission lines are used in [28, 29]. All the reported antennas exhibit multiband characteristic. However, bandwidths of these antennas are not wide enough to cover many

applications, and the structures are complex. The proposed antenna in this paper occupies the wider bandwidth and has simpler geometry, while ensuring the gain and efficiency performance. The proposed antenna structure is simple. It is easy to br fabricated. Moreover, the antenna model is extensible. On the basis of the proposed structure, the antenna can be fractal more times inward for higher frequency and can be fractal outward for lower frequency. Performance comparison of the proposed antenna with other antennas is shown in Table 1.

In this paper, a multiband antenna using a novel circle and triangle structures fractals is proposed and designed for wireless communication systems that can support Bluetooth/WCDMA/CDMA2000/LTE3341WLAN/WiMAX applications. The proposed antenna consists of a main fractal radiator, a 50 Ω microstrip feed line, a ring resonator, and a partial ground plane on the back of the substrate. The proposed antenna shows three distinct resonances with impedance bandwidths of 1.8–2.9 GHz (1.1 GHz), 3.4–4.6 GHz (1.2 GHz), and 5.0–5.6 GHz (0.6 GHz), respectively. The antenna configuration has a compact size of 87.5 mm × 61 mm. The antenna design and studies are described in Section 2. Section 3 includes results and discussion, which are followed by the conclusion in Section 4.

2. Antenna Design and Analysis

Firstly, a triangular gap is nested in a circular radiation patch. This basic geometry is called first-order fractal, as shown in Figure 1(a). The second step is to make an inscribed circle on the triangle gap and nest a triangular gap in the inscribed circle. The rest can be done in the same manner; the antenna radiator adopts four iterations of the square nested triangle slot fractal structure. The final configuration and size parameters of the proposed antenna are shown in Figure 2 and Table 2. In order to make the current flowing through the antenna surface longer, a certain distance d is kept between the circle and the top of the triangle. There is a certain proportion between the dimensions:

$$R_n = \frac{(R_n - d)}{2}, \quad n = 1, 2, 3, \text{ and } 4,$$
$$a_n = \sqrt{3} * (R_n - d), \quad n = 1, 2, \text{ and } 3. \tag{1}$$

By optimizing the antenna radiating slot, the current direction on the metal surface of the microstrip antenna can be changed to achieve multiband coverage. In order to achieve multiband, while improving out band rejection and expanding bandwidth, a resonator ring is designed on the back side of the dielectric board. The current will be coupled to the resonant ring when it flows through the radiator, resulting in disturbing of the current direction and generating multiple resonance frequency points.

Figure 3 shows the reflection coefficient S_{11} of the antenna with different iterations, respectively. For the first and second iteration, S_{11} at the resonance point becomes smaller with the increase of iteration times. For the third iteration, reflection loss characteristics are not improved, but another resonance frequency appears at 4.6 GHz. S_{11} becomes further deeper for the fourth fractal. The antenna property tends to be stable and the best matching status. Compared with the antenna with no resonant ring, the introduction of the resonant ring can improve the reflection coefficient characteristics, increase the resonance points, and effectively expand the bandwidth.

The black solid line presents the simulated reflection coefficient S_{11} of the final proposed antenna. The antenna covers three different frequency bands. At the center frequency, S_{11} is −26 dB at 2.6 GHz, −30 dB at 3.8 GHz, and −15 dB at 5.3 GHz, respectively. The simulated impedance bands with $S_{11} \leq -10$ dB are 46.2% from 1.8 GHz to 3.2 GHz, 31.6% from 3.4 GHz to 4.6 GHz, and 15.1% from 4.9 GHz to 5.7 GHz. These bands can be applied for 2G, 3G, 4G-LTE, Bluetooth, GPS, WLAN, COMPASS, GLONASS, and ISM2.4G.

As shown in Figure 4, current amplitude distribution of the antenna is presented, which illustrates the relationship between resonant frequencies and structure of the antenna. The red part represents strong current, and the blue and green parts represent weak current. Figures 4(a)–4(c) show the surface current at operation frequencies of 2.6 GHz, 3.8 GHz, and 5.3 GHz successively. In Figure 4(a), the current is mainly concentrated in the outer area of the radiator. The color of the middle area and the innermost area is mostly blue. Therefore, it can be understood that the 2.6 GHz resonance occurs due to the first fractal. In Figure 4(b), except for the part red area in the outer, there is also a lot of red in the middle. It is observed that the resonance occurs due to second fractal. The third resonant mode of the antenna, by considering the current distribution of the antenna as shown in Figure 4(c), arises from the currents in the inner area owing to the third fractal. Based on the above analysis, the current flows from outside to inside with the frequency increasing. According to $f = c/\lambda$, it can be known that the small size of the antenna produces high radiation frequency. Therefore, the resonance frequency generated by the inner ring is higher than the resonance frequency generated by the outer ring.

For the first resonance at 2.6 GHz, the maxima of the current occur in the outer ring. The length of the radiating patch responsible for first resonance can be calculated as

$$L_1 \approx 2 * \pi * R_4 * \frac{1}{3} \approx 50.24 \text{ mm}. \tag{2}$$

At the resonance, the length would be half of the wavelength. L_1 should be $\lambda/2$. For the printed antenna, half of it is on the media plate and the other half is in the air. The calculated wavelength should be between the medium wavelength and the free space wavelength. We take the intermediate value as the estimation temporarily to verify the rationality of the fractal design.

Therefore,

$$f_1 \approx \frac{1}{2} * \left(\frac{c}{2L_1\sqrt{\varepsilon_r}} + \frac{c}{2L_1} \right) \approx 2.2 \text{ GHz}. \tag{3}$$

For the second resonance at 3.8 GHz, the maxima of the current occur in the middle ring. The length of the radiating patch responsible for second resonance can be calculated as

Table 1: Performance comparison of the proposed antenna with other antennas.

Ref.	Bands (GHz)	Gain (dBi)	Efficiency
[22]	2.0–2.76, 3.04–4.0, 5.2–6.0, and 5.2–5.8	1.5–3.05	87%–95%
[23]	2.21–4.40 and 5.13–5.55	0.5–2	66%–72%
[24]	1.71–2.03 and 5.02–5.28	3.5–7	60%–80%
[25]	2.2–2.9, 3.2–4.7, and 4.8–6.6	0-1	—
[26]	2.39–2.51, 3.15–3.91, and 4.91–6.08	1.6–2.8	—
[27]	2–2.15, 2.75–3.52, and 5.4–5.9	—	40%–70%
[28]	2.3–4 and 5–6.6	2.3–3.2	61.7%–76.5%
[29]	2.42–3.51	2.1	96.5%
Proposed	1.8–2.9, 3.4–4.6, and 5–5.6	2.58–3.34	75.8%–95.0%

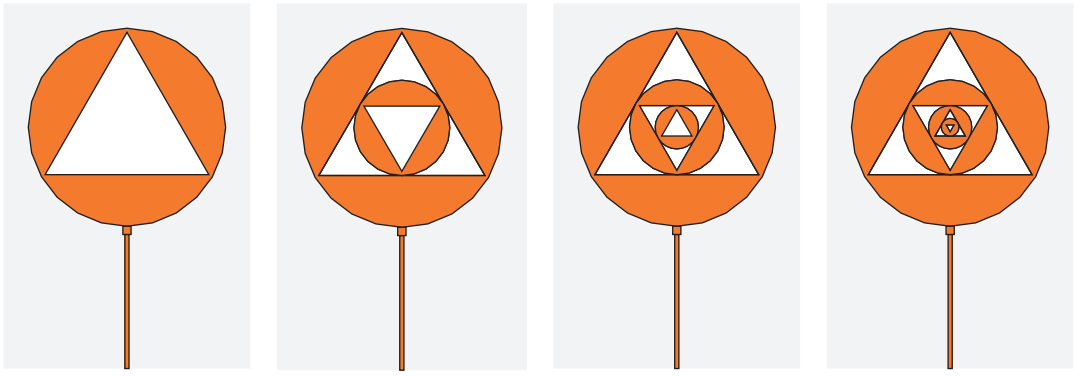

Figure 1: Fractal progress.

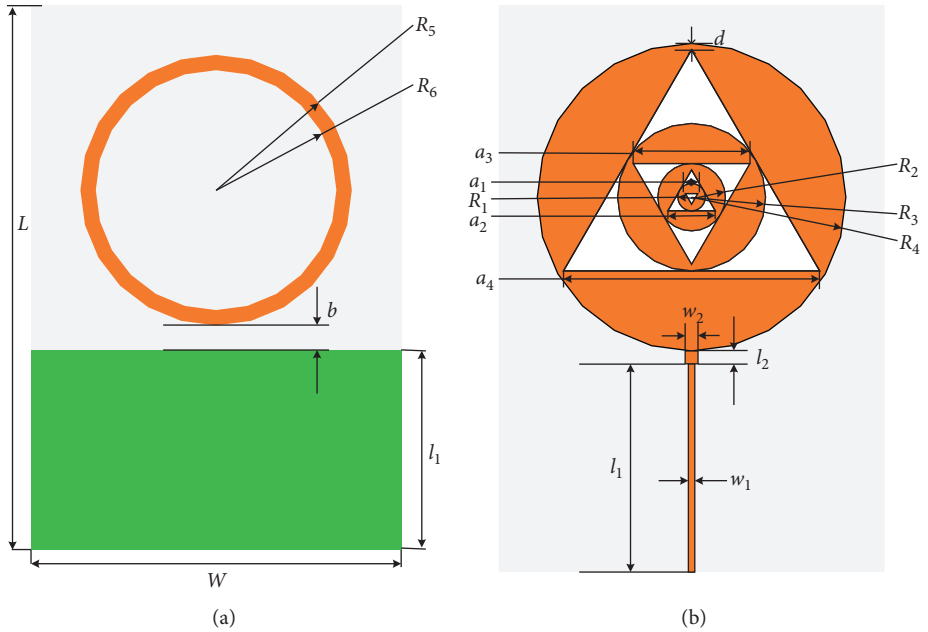

Figure 2: The configuration of the antenna: (a) bottom view; (b) top view.

Table 2: The dimensions of the proposed antenna.

Parameter	Values (mm)
W	61
w_1	1
w_2	2
R_1	2.125
R_3	11.5
R_5	22
a_1	1.95
a_3	18.19
b	4
L	87.5
l_1	32.5
l_2	2
R_2	5.25
R_4	24
R_6	19.5
a_2	7.36
a_4	39.84
d	1

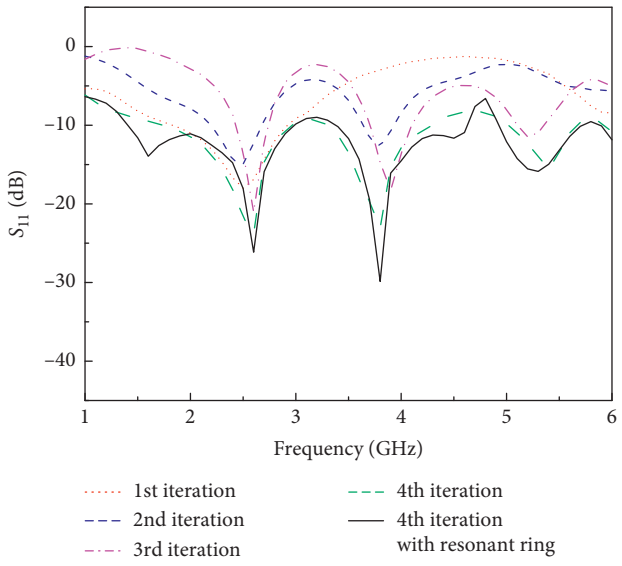

Figure 3: The simulated S_{11} for the antenna iterations.

$$L_2 \approx 2 * \pi * R_3 * \frac{1}{3} \approx 24.07\,\text{mm},$$
$$f_2 \approx \frac{1}{2} * \left(\frac{c}{2L_2\sqrt{\varepsilon_r}} + \frac{c}{2L_2}\right) \approx 4.5\,\text{GHz}. \quad (4)$$

For the third resonance at 5.3 GHz, the maxima of the current occur in the inner ring. The length of the radiating patch responsible for third resonance can be calculated as

$$L_3 \approx 2 * \pi * R_2 * \frac{2}{3} \approx 21.98\,\text{mm},$$
$$f_3 \approx \frac{1}{2} * \left(\frac{c}{2L_3\sqrt{\varepsilon_r}} + \frac{c}{2L_3}\right) \approx 5.0\,\text{GHz}. \quad (5)$$

The 3D pattern of the designed antenna is shown in Figure 5, and the E/H plane polarization is shown in Figure 6. The blue solid line represents coplanar polarization, and the red dotted line represents cross polarization. It can be seen from the figure that the three-dimensional spatial radiation field at three resonance points has certain changes. With the increase of the resonance frequency, the radiation directivity of the antenna becomes stronger. The main lobe becomes smaller, weak side lobes appear, and directivity becomes complicated. The maximum gain can achieve 3.33 dBi, 3.82 dBi, and 5.77 dBi at central frequencies of 2.6 GHz, 3.8 GHz, and 5.3 GHz, respectively.

3. Results and Discussion

The proposed multiband antenna is manufactured on a 1.6 mm thick FR4 substrate with a dielectric constant of 4.4 and a loss tangent of 0.02. The copper with 0.03 mm thick is laid over the patch and ground plane. The prototype of the fabricated antenna is shown in Figure 7.

The Keysight Technologies FieldFox Handheld Microwave Analyzer N9917A is used to measure the reflection coefficient of the fabricated antenna. Figure 8 illustrates the comparison of simulated and measured results. The measured −10 dB bandwidth is 42.5% from 1.8 GHz to 2.9 GHz, 30% from 3.4 GHz to 4.6 GHz, and 5.3% from 5 GHz to 5.6 GHz, which is in good agreement with the simulation result. The commercial band coverage is shown in Table 3. Slight discrepancies between measurement and simulation results may be caused by fabrication precision, interface error, and test environment. The substrate thickness of the antenna is only 1.6 mm, and the influence of the dielectric thickness change during the processing on the performance of the antenna cannot be ignored. The connection method of SMA between the feeder and the signal is solder connection. The solder increases the thickness of the dielectric board, which has a certain impact on the test results. The error is within the allowable range.

Figure 9 displays the measured 3D radiation patterns at central frequency of 2.5 GHz, 3.8 GHz, and 5.3 GHz, respectively. The pick gain can achieve 2.98 dBi, 2.58 dBi, and 3.34 dBi at frequencies of 2.5 GHz, 3.8 GHz, and 5.3 GHz, respectively. The measured radiation patterns are nearly omnidirectional. With the frequency increasing, the generation of higher order modes increases the side lobes.

Gain and efficiency variation with the frequency is shown in Figure 10. It is found that the gain varies from 1.9 to 4.1 dBi in I band, from 0.5 to 4.0 dBi in II band, and from 1.2 to 3.3 dBi in III band. The radiation efficiency of the antenna can achieve 92.5%, 75.5%, and 95.0% at central frequency of 2.5 GHz, 3.8 GHz, and 5.3 GHz. The test results are consistent with the simulation results basically. However, when testing the antenna pattern in the dark room, it is inevitable to connect the antenna to the test equipment with radio frequency cables and connectors. These RF cables and connectors are very close to the antenna, and their radiation will affect the pattern test. Therefore, it is inevitable that there is a certain deviation between the test results and the simulation results.

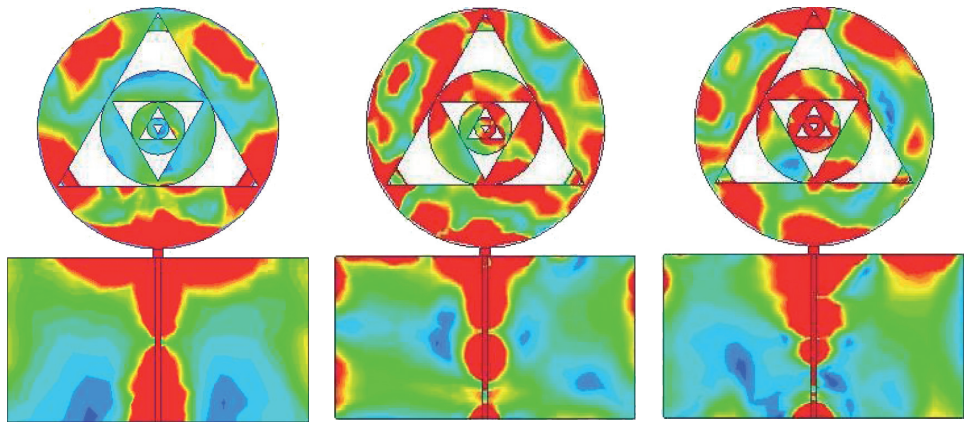

(a) (b) (c)

Figure 4: Current amplitude and vector distribution of the antenna at (a) 2.6 GHz, (b) 3.8 GHz, and (c) 5.3 GHz.

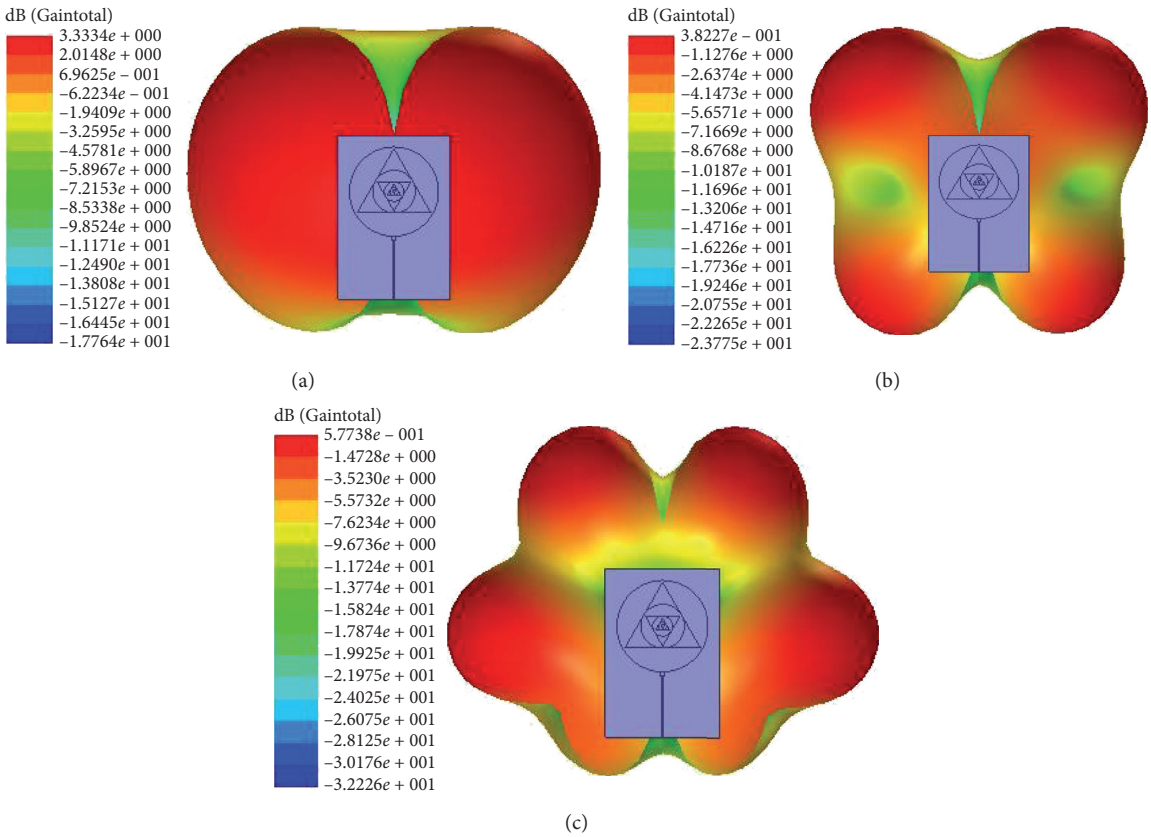

(a) (b) (c)

Figure 5: 3D radiation pattern at (a) 2.6 GHz, (b) 3.8 GHz, and (c) 5.3 GHz.

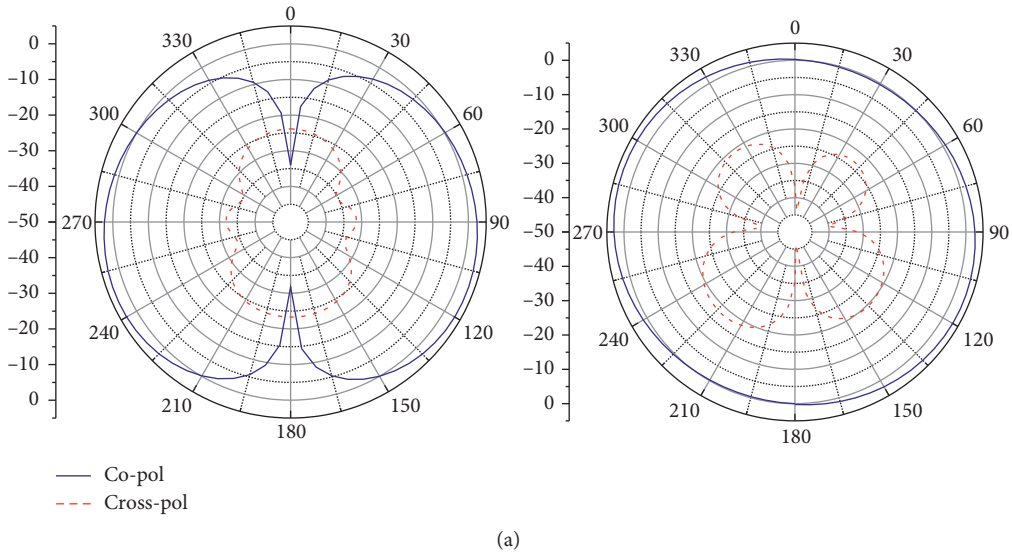

(a)

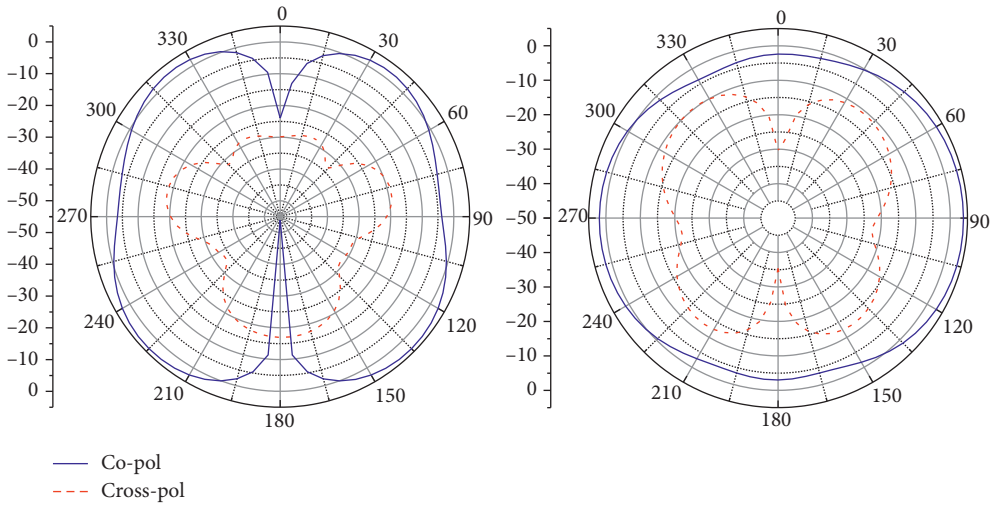

(b)

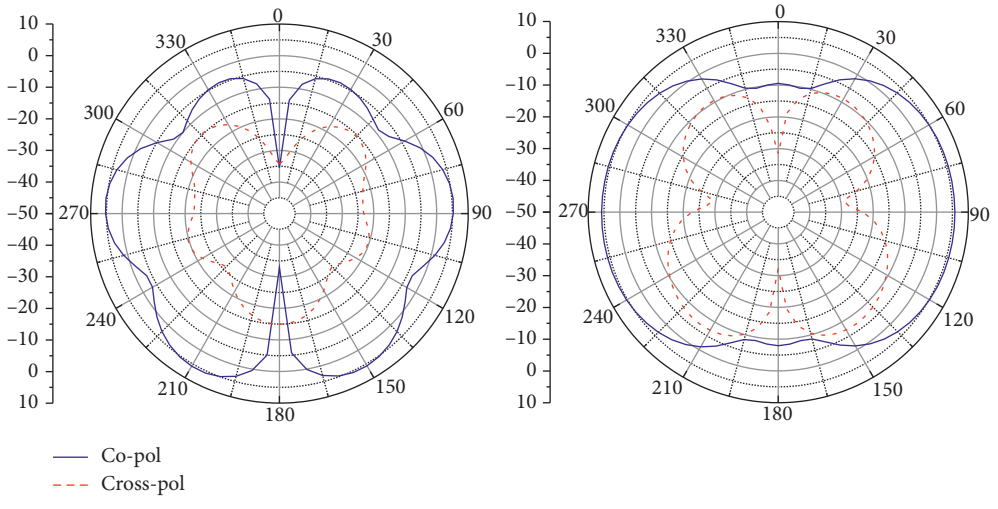

(c)

Figure 6: E/H plane polarization. (a) 2.6 GHz. (b) 3.8 GHz. (c) 5.3 GHz.

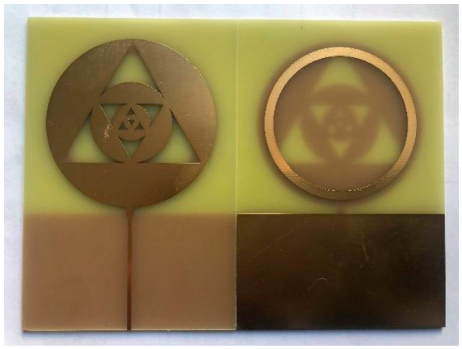

Figure 7: The configuration of the proposed antenna.

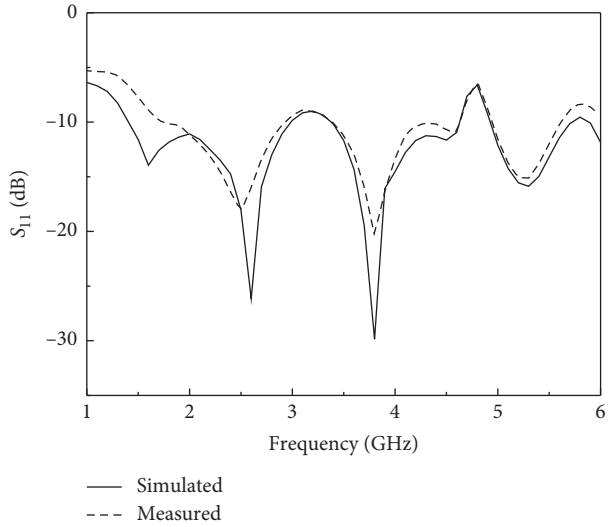

Figure 8: The comparison of simulated and measured S_{11}.

Table 3: Commercial band coverage by the designed antenna.

Frequency band	Bandwith	Commercial band coverage
1	1.8–2.9 GHz (42.5%)	TD-SCDMA (1880–2025 MHz) WCDMA (1920–2170 MHz) CDMA2000 (1920–2125 MHz) LTE33-41 (1900–2690 MHz) Bluetooth
2	3.4–4.6 GHz (30%)	LTE42/43 (3.4–3.8 GHz) WiMAX (3.3–3.8 GHz)
3	5.0–5.6 GHz (11.3%)	WLAN (802.11a/n:5.15–5.35 GHz)

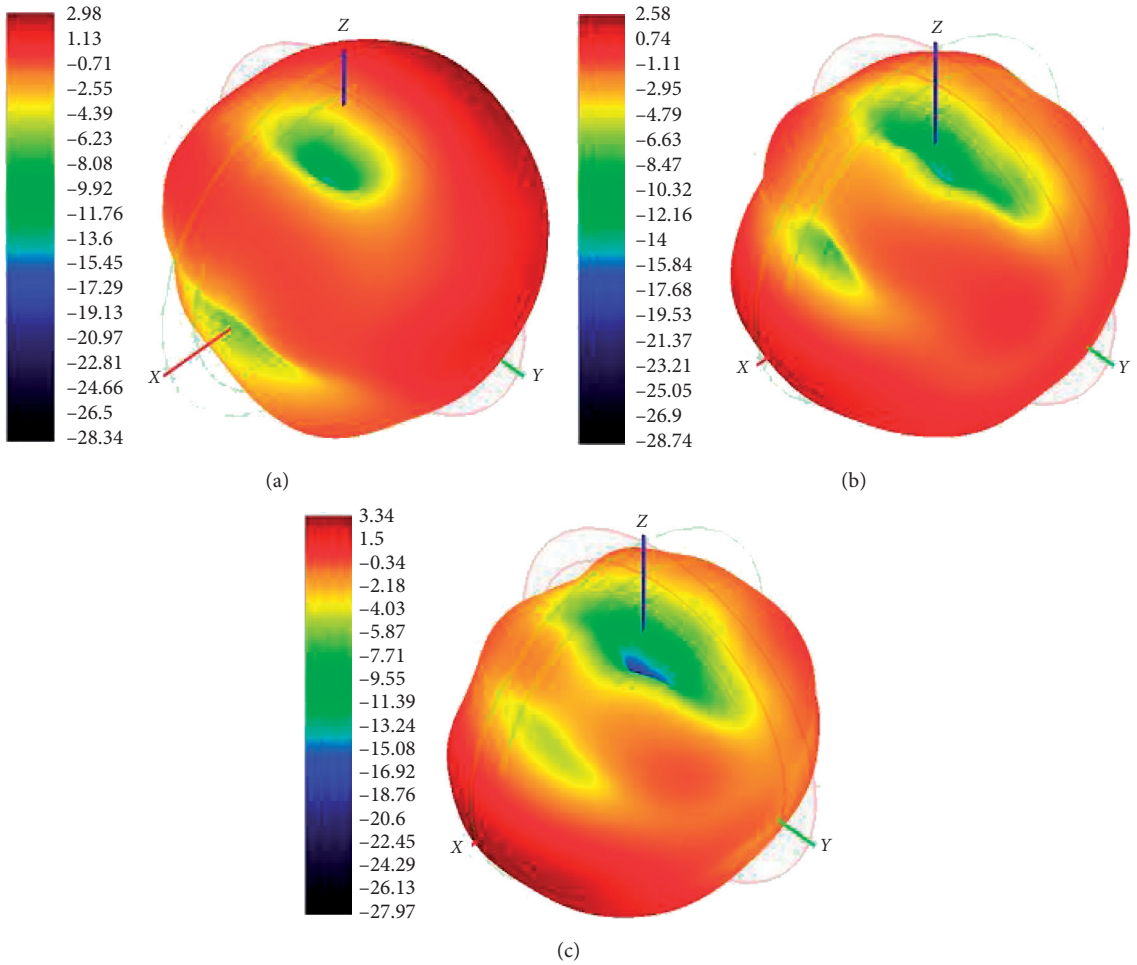

Figure 9: The measured 3D pattern. (a) 2.5 GHz. (b) 3.8 GHz. (c) 5.3 GHz.

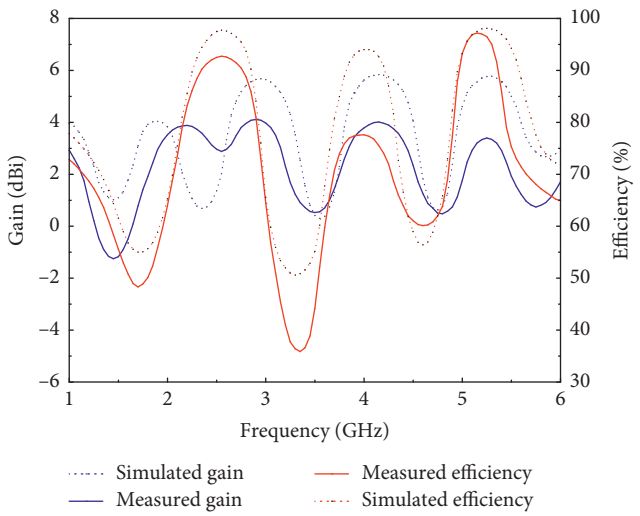

Figure 10: Gain and efficiency of the antenna.

4. Conclusion

In this paper, an optimal microstrip-fed printed antenna with a novel circular nested triangle slotting multiband fractal is successfully proposed, simulated, and fabricated. The antenna consists of four parts, including a main fractal radiator, a 50 Ω microstrip feed line, a ring resonator, and a partial ground plane on the back of the substrate. The antenna is designed on a single-layer FR4 and covers the frequency of 1.8 GHz–2.9 GHz, 3.4 GHz–4.6 GHz, and 5 GHz–5.6 GHz. Experiments are carried out to validate the design concept and method, showing good agreement between simulations and measurements. At all frequency bands, the proposed antenna features stable radiation performance indicating that it can be a good candidate for Bluetooth, TD-SCDMA, WCDMA, CDMA2000, LTE33-41, WLAN, and WiMAX applications.

Data Availability

The data used to support the findings of this study are included within the article.

Conflicts of Interest

The authors declare that they have no conflicts of interest.

Acknowledgments

This work was supported by the National Natural Science Foundation of China (nos. 61531007 and 61821001).

References

[1] S. Singhal, P. Singh, and A. Kumar Singh, "Asymmetrically CPW-fed octagonal sierpinski UWB fractal antenna," *Microwave and Optical Technology Letters*, vol. 58, no. 7, pp. 1738–1745, 2016.

[2] T. Nguyen-Trung, Y. Yang, K.-Y. Lee, and K. C. Hwang, "Dual circularly-polarized spidron fractal slot antenna," *Electromagnetics*, vol. 37, no. 1, pp. 40–48, 2017.

[3] R. K. Yadav, J. Kishor, and R. L. Yadava, "A chaucer microstrip fractal antenna for mobile applications," *Journal of Communications Technology and Electronics*, vol. 61, no. 2, pp. 138–144, 2016.

[4] K.-L. Wong and L.-C. Lee, "Multiband printed monopole slot antenna for WWAN operation in the laptop computer," *IEEE Transactions on Antennas and Propagation*, vol. 57, no. 2, pp. 324–330, 2009.

[5] Y.-S. Shin, B.-N. Kim, and W. I. Seong-Ook Park, "GSM/DCS/IMT-2000 triple-band built-in antenna for wireless terminals," *IEEE Antennas and Wireless Propagation Letters*, vol. 3, no. 1, pp. 104–107, 2004.

[6] W. J. Krzysztofik, "Modified sierpinski fractal monopole for ISM-bands handset applications," *IEEE Transactions on Antennas and Propagation*, vol. 57, no. 3, pp. 606–615, 2009.

[7] C.-J. Wang and K.-L. Hsiao, "CPW-fed monopole antenna for multiple system integration," *IEEE Transactions on Antennas and Propagation*, vol. 62, no. 2, pp. 1007–1011, 2014.

[8] K. Yu, Y. S. Li, W. H. Yu et al., "A compact triple band antenna for bluetooth,WLAN and WiMAX applications," *Applied Computational Electromagnetics Society Journal*, vol. 32, no. 5, pp. 424–429, 2017.

[9] H. Oraizi and S. Hedayati, "Circularly polarized multiband microstrip antenna using the square and giuseppe peano fractals," *IEEE Transactions on Antennas and Propagation*, vol. 60, no. 7, pp. 3466–3470, 2012.

[10] P. S. Bakariya, S. Dwari, M. Sarkar, and M. K. Mandal, "Proximity-coupled microstrip antenna for bluetooth, WiMAX, and WLAN applications," *IEEE Antennas and Wireless Propagation Letters*, vol. 14, pp. 755–758, 2015.

[11] S. C. Basaran, U. Olgun, and K. Sertel, "Multiband monopole antenna with complementary split-ring resonators for WLAN and WiMAX applications," *Electronics Letters*, vol. 49, no. 10, pp. 636–638, 2013.

[12] J. H. Yoon, Y. C. Rhee, and Y. K. Jang, "Compact monopole antenna design for WLAN/WIMAX triple-band operations," *Microwave and Optical Technology Letters*, vol. 54, no. 8, pp. 1838–1846, 2012.

[13] L. Kumar, A. Gautam, B. Kanaujia et al., "Design of compact F-shaped slot triple band antenna for WLAN/WiMAX applications," *IEEE Transactions on Antennas & Propagation*, vol. 64, no. 3, pp. 1101–1105, 2016.

[14] W. Hu, Y.-Z. Yin, and P. Xi Yang, "Compact triband square-slot antenna with symmetrical L-strips for WLAN/WiMAX applications," *IEEE Antennas and Wireless Propagation Letters*, vol. 10, pp. 462–465, 2011.

[15] A. Kunwar, A. K. Gautam, and B. K. Kanaujia, "Inverted L-slot triple-band antenna with defected ground structure for WLAN and WiMAX applications," *International Journal of Microwave and Wireless Technologies*, vol. 9, no. 1, pp. 191–196, 2017.

[16] A. Foudazi, H. R. Hassani, and S. Mohammad Ali Nezhad, "Small UWB planar monopole antenna with added GPS/GSM/WLAN bands," *IEEE Transactions on Antennas and Propagation*, vol. 60, no. 6, pp. 2987–2992, 2012.

[17] M. Rafaei Booket, A. Jafargholi, M. Kamyab et al., "Compact multi-band printed dipole antenna loaded with single-cell metamaterial," *IET Microwaves, Antennas & Propagation*, vol. 6, no. 1, pp. 12–23, 2012.

[18] M. Tzortzakakis and R. J. Langley, "Quad-band internal mobile phone antenna," *IEEE Transactions on Antennas and Propagation*, vol. 55, no. 7, pp. 2097–2103, 2007.

[19] H. W. Hsieh, Y.-C. Lee, K.-K. Tiong, and J.-S. Sun, "Design of a multiband antenna for mobile handset operations," *IEEE Antennas and Wireless Propagation Letters*, vol. 8, pp. 200–203, 2009.

[20] M. Naghshvarian Jahromi, A. Falahati, R. M. Edwards et al., "Bandwidth and impedance-matching enhancement of fractal monopole antennas using compact grounded coplanar waveguide," *IEEE Transactions on Antennas and Propagation*, vol. 59, no. 7, pp. 2480–2487, 2011.

[21] S. Dhar, K. Patra, R. Ghatak, B. Gupta, and D. R. Poddar, "A dielectric resonator-loaded minkowski fractal-shaped slot loop heptaband Antenna," *IEEE Transactions on Antennas and Propagation*, vol. 63, no. 4, pp. 1521–1529, 2015.

[22] A. K. Gautam, L. Kumar, B. K. Kanaujia, and K. Rambabu, "Design of compact F-shaped slot triple-band antenna for WLAN/WiMAX applications," *IEEE Transactions on Antennas and Propagation*, vol. 64, no. 3, pp. 1101–1105, 2016.

[23] G. Augustin and T. A. Denidni, "Coplanar waveguide-fed uniplanar trapezoidal antenna with linear and circular polarization," *IEEE Transactions on Antennas and Propagation*, vol. 60, no. 5, pp. 2522–2526, 2012.

[24] D. Li and J.-f. Mao, "A koch-like sided fractal bow-tie dipole antenna," *IEEE Transactions on Antennas and Propagation*, vol. 60, no. 5, pp. 2242–2251, 2012.

[25] X. Liu, M. M. Tentzeris, and S. H. Zheng, "Optically controlled reconfigurable band-notched UWB antenna for cognitive radio systems," *Electronics Letters*, vol. 50, no. 21, pp. 1502–1504, 2014.

[26] A. Kunwar, A. K. Gautam, and B. K. Kanaujia, "Inverted L-slot triple-band antenna with defected ground structure for WLAN and WiMAX applications," *International Journal of Microwave and Wireless Technologies*, vol. 9, no. 1, pp. 191–196, 2017.

[27] S. Joshi, A. K. Gautam, and R. Upadhyay, "Frequency agile triple band microstrip antenna for WLAN/WiMAX application," *International Journal of Future Computer and Communication*, vol. 3, no. 4, pp. 258–261, 2014.

[28] H. Huang, Y. Liu, S. Zhang, and S. Gong, "Multiband metamaterial-loaded monopole antenna for WLAN/WiMAX applications," *IEEE Antennas and Wireless Propagation Letters*, vol. 14, pp. 662–665, 2015.

[29] C. Zhou, G. Wang, J. Liang, Y. Wang, and B. Zong, "Broadband antenna employing simplified MTLs for WLAN/WiMAX applications," *IEEE Antennas and Wireless Propagation Letters*, vol. 13, pp. 595–598, 2014.